Mecánica Computacional Vol. XXI, pp. 541–565
S. R. Idelsohn, V. E. Sonzogni and A. Cardona (Eds.)
Santa Fe–Paraná, Argentina, October 2002

NUMERICAL MODELING OF FLOW AND MASS TRANSFER IN BUBBLE PLUMES

Gustavo C. Buscaglia*, Enzo A. Dari*, Fabián A. Bombardelli†, and Marcelo H. García†

*Centro Atómico Bariloche and Instituto Balseiro
8400 Bariloche, Argentina
e-mail: gustavo@cab.cnea.gov.ar, web page: http://cabmec1.cnea.gov.ar/gustavo

†Ven Te Chow Hydrosystems Laboratory, Dept. of Civil and Environm. Eng.
University of Illinois at Urbana-Champaign, Urbana, IL 61801, USA
e-mail: mhgarcia@uiuc.edu, web page: http://cee.uiuc.edu/hydro

Key Words: Two-phase flow, bubble plumes, two-fluid equations, finite elements.

Abstract. *A mathematical model for dilute bubble plumes is derived from the two-fluid model equations. This is coupled to a mass transfer model to get a closed CFD formulation. The mass transfer equations used are those implemented in the 1D integral model proposed by Wüest* et al *(*Water Resources Research*, 28:3235-3250, 1992). Integral formulations are widely used in hydraulics, and it is interesting to build a CFD formulation which is based on (and fully consistent with) one of them.*

The model is tested for typical conditions of isolated aeration plumes in deep wastewater reservoirs and the results compared to those of the integral model. Good agreement is observed, especially in the most relevant variables such as gas dissolution rates, gas holdup, liquid's velocity and bubbles' radius. Furthermore, entrainment rates evaluated from the CFD results are shown to lie within the experimental range. A solid justification for applying CFD models to aeration plumes, as natural extensions of the popular integral models, emerges from the investigation.

We then report two additional numerical examples. The first concerns a bubble plume in an experimental tank, and the aim is to assess the effect of the different forces (lift, virtual mass and turbulent dispersion in particular). The second is a constrained bubble plume which spontaneously bifurcates into a quasi-periodic motion and has challenged several approximation schemes in the last years.

1 INTRODUCTION

Air-bubble plumes have numerous applications such as pneumatic breakwaters, antifreeze measures, silt curtains, and barriers to contain density intrusions or oil spills.[1–4] For deep water bodies (lakes, reservoirs) injection of air-bubbles is often used for destratification of the water volume.[5–7] In wastewater treatment aeration with bubble plumes has been employed for about a century,[8] however its use in deep reservoirs containing biochemically active water is an emerging application. The construction of large wastewater reservoirs is being motivated by environmental concerns. The idea is to provide storage for combined sewage and stormwater during big storms, so that water treatment plants can operate in batch mode. This is an important problem in large metropolitan areas such as Chicago, Illinois.

Power efficiency in aeration devices for deep water bodies is essential due to the high injection pressure needed. Design optimization with sound scientific tools is thus in order, and numerical modeling is without doubt one of the key tools in all fields of engineering. In plume modeling simulation codes have mostly used the transversally-integrated equations,[5–7,9–11] based on a self-similarity assumption and the well-known entrainment hypothesis.[12] The problem is thus reduced to just one spatial dimension, at the cost of introducing some heuristic coefficients that must be obtained from experiments.

A transversally-integrated model (frequently referred to as *integral model*) that accounts for most of the physical and chemical processes related to aeration of reservoirs was introduced by Wüest *et al*[11] to help in the design of lake restoration systems. The aim of the present article is to extend that model in a systematic way to two-fluid flow modeling and computational fluid dynamics (CFD). An improved formulation results which has less empirical coefficients and can deal with arbitrary geometries. Moreover, wastewater reservoir aeration involves the simultaneous operation of many bubble plumes. While integral models assume the plume to be isolated, CFD formulations are the appropriate tool to study plume-plume, plume-boundary and plume-crossflow interactions.

The two-fluid model proposed here is based on the general theory of multiphase flows[13] and has three main components:

- A hydrodynamical component that considers the main physical processes in a free dilute bubbly flow.
- A mass-transfer component that considers oxygen and nitrogen dissolution from the bubbles and was taken from Wüest *et al* (1992).[11]
- A liquid chemistry component that incorporates a basic water-quality model taken from the book by Chapra.[14] The variables are dissolved oxygen concentration, dissolved nitrogen concentration, and the biochemical oxygen demand that encompasses all oxygen-consuming processes.

The organization of the paper is as follows: In Section 2 a mathematical model for dilute bubbly flows is described and justified in which the mass exchange between liquid

and gas, together with a basic water-quality model, are incorporated. Section 3 describes the numerical treatment of the model equations in the CFD code. Section 4 contains several numerical results. We first compare the CFD results with those of an integral model, obtaining excellent agreement. We then assess the effect of the different forces (virtual mass, lift, turbulent dispersion). Finally, we show a three-dimensional example in which the bubble plume exhibits spontaneous oscillations, which has challenged several numerical schemes in the last years. The most relevant conclusions are drawn in Section 5.

2 MATHEMATICAL MODEL

2.1 Two-fluid model and dynamical equations

The two-fluid model can be obtained by ensemble-averaging the exact conservation equations for each phase in a multiphase flow.[13] Let $X_k(x,t;\nu)$ be the *component indicator function*, which for a given realization ν of the flow takes the value one if phase k is present at point x at time t, and takes the value zero otherwise. The following averaged quantities are needed to write down the equations:

- $\alpha_k = \overline{X}_k$, is the so-called volume fraction of phase k but is, in fact, the *probability* of phase k.
- The averaged density and velocity of phase k are defined by

$$\overline{\rho}_k = \frac{\overline{X_k \rho}}{\alpha_k}; \qquad \overline{u}_k = \frac{\overline{X_k \rho u}}{\alpha_k \overline{\rho}_k}. \tag{1}$$

- The pressure, on the other hand, is not mass averaged,

$$\overline{p}_k = \frac{\overline{X_k p}}{\alpha_k} \tag{2}$$

We neglect pressure differences between the phases ($\overline{p}_k = \overline{p},\ \forall\, k$) and the shear stresses at the interphase. We denote by Γ_k the interphase mass transfer rate ($\sum_k \Gamma_k = 0$) and neglect the momentum transfer arising from mass transfer between the phases. One ends up with the following averaged equations for phase k:

$$\frac{\partial \alpha_k \overline{\rho}_k}{\partial t} + div\ (\alpha_k \overline{\rho}_k \overline{u}_k) \;=\; \Gamma_k \tag{3}$$

$$\frac{\partial\, \alpha_k \overline{\rho}_k \overline{u}_k}{\partial t} + div\ (\alpha_k \overline{\rho}_k \overline{u}_k \otimes \overline{u}_k) + \alpha_k\, \nabla \overline{p} \;=\; div\ \left(\alpha_k \overline{T}_k\right) - \alpha_k \overline{\rho}_k g\, \mathbf{k} + M'_k \tag{4}$$

where the effective stress $\overline{T}_k$ contains both the averaged deviatoric stresses of phase k and the fluctuation stress tensor that arises from the inertia term along the averaging

process.[13] Here $\mathbf{k}$ is the upwards vertical unit vector and g is the acceleration of gravity. The interfacial forces such as drag, lift, etc. are contained in M'_k, with $\sum_k M'_k = 0$.

The averaged equations implemented in our code consider a liquid phase ($k = \ell$) and a gaseous phase ($k = g$). We will make use of the *mixture* equations, which are obtained by adding up the balance equations of the individual phases. Let us define the mixture quantities as:

$$\rho_m = \alpha_\ell \overline{\rho}_\ell + \alpha_g \overline{\rho}_g \tag{5}$$

$$\rho_m u_m = \alpha_\ell \overline{\rho}_\ell \overline{u}_\ell + \alpha_g \overline{\rho}_g \overline{u}_g \tag{6}$$

$$T_m = \alpha_\ell \overline{T}_\ell + \alpha_g \overline{T}_g \tag{7}$$

$$p_m = \overline{p} \tag{8}$$

Then, from (3)-(4) it follows that

$$\frac{\partial \rho_m}{\partial t} + div\ (\rho_m u_m) = 0 \tag{9}$$

$$\frac{\partial \rho_m u_m}{\partial t} + div\ (\rho_m u_m \otimes u_m) + \nabla p_m = div\, T_m - \rho_m g\, \mathbf{k} - div\ \left[\sum_k \alpha_k \overline{\rho}_k \left(\overline{u}_k - u_m\right) \otimes \left(\overline{u}_k - u_m\right) \right] \tag{10}$$

Let us define the relative velocity between the phases as $u_r = \overline{u}_g - \overline{u}_\ell$, so that the summation in the last term of (10) satisfies

$$\sum_k \alpha_k \overline{\rho}_k \left(\overline{u}_k - u_m\right) \otimes \left(\overline{u}_k - u_m\right) = \alpha_g \overline{\rho}_g \left(1 - \frac{\alpha_g \overline{\rho}_g}{\rho_m}\right) u_r \otimes u_r \tag{11}$$

This term is neglected in the following since both α_g and $\overline{\rho}_g / \rho_m$ are assumed to be much smaller than unity, while u_r and u_m are of the same order.

Notice that

$$\rho_m = \overline{\rho}_\ell - \alpha_g \left(\overline{\rho}_\ell - \overline{\rho}_g\right) \ , \tag{12}$$

so that $\rho_m - \overline{\rho}_\ell \simeq -\alpha_g \overline{\rho}_\ell$. Assuming the liquid phase to be incompressible, we can now adopt the Boussinesq approximation replacing ρ_m by $\overline{\rho}_\ell$ in all terms but the gravity one. This approximation is routinely applied in thermal problems with temperature differences as high as 20° C (in water), so that one can expect it to hold for values of α_g leading to the same magnitude of density change, i.e., $\alpha_g < 10^{-2}$. The model as a whole is quite simple but as shown above follow from the two-fluid model under reasonable hypotheses. This is further discussed elsewhere.[15]

2.2 Adopted CFD formulation

Assuming in the mixture equations (9)-(10) that the stress tensor T_m is dominated by turbulent stress, adopting a $k-\epsilon$ model for the turbulence closure and modifying the pressure as $\hat{p}_m = p_m + \frac{2}{3}k$ the final equations are

$$div\, u_m = -\frac{1}{\rho^*}\left(\frac{\partial \rho^*}{\partial t} + u_m \cdot \nabla \rho^*\right) \tag{13}$$

$$\rho^* \frac{\partial u_m}{\partial t} + \rho^* \left(u_m \cdot \nabla\right) u_m + \nabla \hat{p}_m = div\, \left[\mu_T \left(\nabla u_m + \nabla^T u_m\right)\right] - \rho_m g\, \mathbf{k} \tag{14}$$

$$\mu_T = \rho^* C_\mu \frac{k^2}{\epsilon} \tag{15}$$

where $C_\mu = 0.09$ and, to add generality to the formulation, ρ^* may be taken as ρ_ℓ (Boussinesq approximation) or as ρ_m. The equations for k and ϵ, together with the treatment of wall laws, correspond to the standard model (see, e.g., the book by Wilcox;[16] our implementation is presented by Lew *et al*[17]). No corrections for bubble-induced turbulence are performed.

This certainly deserves a comment. Several corrections to the $k-\epsilon$ equations to account for the effect of bubbles have been proposed. A popular one is due to Sato *et al*,[18] who add $1.2\rho_0 r_b \alpha_g |u_r|$ to the eddy viscosity, where r_b is the bubble radius. Typical values obtained for μ_T are above 10 Pa-s, while usual values are $r_b = 2\times 10^{-3}$ m, $|u_r| = 0.3$ m/s and $\alpha_g < 10^{-2}$. The correction would thus be smaller than 10^{-2} Pa-s, which can clearly be neglected.

Mudde & Simonin[19] applied a $k-\epsilon$ model with quite elaborate corrections proposed by Viollet & Simonin[20] to simulate the plume-wandering experiments of Becker *et al*.[21] Only after adding virtual-mass effects did they get agreement with the experimental data. However, the 3D simulations of Sokolichin & Eigenberger[22] and of Borchers *et al*[23] with the *standard* $k-\epsilon$ model (and a constant bubble-slip velocity!) show excellent agreement. Similar agreement was also obtained by Pfleger *et al*[24] with again the standard model but a drag law to calculate bubble-slip velocity. Smith,[25] on the other hand, concludes that the corrections of Viollet & Simonin[20] do bring some improvement, while those of Malin & Spalding[26] lead to incorrect results. We show in Section 4 that for Becker's experiment our model correctly predicts the observed spontaneous oscillations, thus validating to some extent the approach in a dynamical case. Also notice that the standard $k-\epsilon$ model has also been favored by many other authors.[27–31]

2.3 The basic gas-phase model

The gas-phase model of Wüest *et al*[11] is quite simple. No bubble coalescence or breakup is accounted for, so that the (averaged) number of bubbles per unit volume N_b satisfies

$$\frac{\partial N_b}{\partial t} + div\ (N_b u_g) = div\ (\mathcal{D}_g \nabla N_b) \tag{16}$$

and the bubbles are assumed to have a unimodal size distribution.

The model also assumes a bubble-slip velocity that only depends on the bubble radius, i.e.,

$$u_g = u_m + w_b(r_b)\,\mathbf{k}, \text{ with } w_b = \begin{cases} 4474\frac{m}{s} \times r_b^{1.357} & \text{if } 0 \le r_b \le 7\times 10^{-4}m \\ 0.23\frac{m}{s} & \text{if } 7\times 10^{-4}m < r_b \le 5.1\times 10^{-3}m \\ 4.202\frac{m}{s} \times r_b^{0.547} & \text{if } r_b > 5.1\times 10^{-3}m \end{cases} \tag{17}$$

where r_b is expressed in meters. The velocity law is a fit to data presented by Haberman & Morton.[32] A thorough presentation of terminal velocities of bubbles in water can be found in the book by Clift *et al.*[33]

In (16) we have incorporated a dispersion coefficient $\mathcal{D}_g$ which as proposed by Carrica *et al*[34] results from

$$\mathcal{D}_g = \frac{\mu_T}{\rho_\ell Sc_g} \tag{18}$$

with the Schmidt number for the gas Sc_g taken equal to one. Moraga *et al*[35] recommend 0.83 for very small bubbles (small Stokes numbers), but it is expected to increase for larger ones.

Finally, the gas concentration equations are introduced. We consider the gas to consist basically of two species, gaseous nitrogen and gaseous oxygen, and we introduce the molar concentrations C_N and C_O, defined as the number of moles of each gas *per unit volume of mixture*. The following relations are elementary ($\mathcal{R}$ is the universal gas constant, 8.314 J/mol-K, T_g is the absolute gas temperature, assumed known, $\mathcal{M}_N$ and $\mathcal{M}_O$ refer to the molecular weights of N_2, 28 kg/kmol, and O_2, 32 kg/kmol)

$$\alpha_g = \frac{\mathcal{R}T_g(C_N + C_O)}{p_g} \tag{19}$$

$$\rho_g = \frac{C_N\mathcal{M}_N + C_O\mathcal{M}_O}{\alpha_g} \tag{20}$$

The pressure of the gas is assumed to obey $\rho_0 g(H + H_a - z)$, where H is the maximum depth, H_a the atmospheric head, and z the vertical coordinate measured from the point of maximum depth. Surface tension effects are thus not modeled in the present version, but could easily be added. It is unlikely that non-hydrostatic effects be significant in any environmental plume, but would not represent a major difficulty either.

Mass balance of each species leads to

$$\frac{\partial C_O}{\partial t} + div\ (C_O\, u_g) = \mathcal{S}_O + div\ \left(\frac{\mu_T}{\rho_\ell Sc_g}\nabla C_O\right) \tag{21}$$

$$\frac{\partial C_N}{\partial t} + div\ (C_N\, u_g) = \mathcal{S}_N + div\ \left(\frac{\mu_T}{\rho_\ell Sc_g}\nabla C_N\right) \tag{22}$$

where $\mathcal{S}_O$ and $\mathcal{S}_N$ are mass source terms that arise from the chemical interaction (dissolution) of the gas in the surrounding fluid, to be discussed in the next subsection. Notice that $\mathcal{M}_O\mathcal{S}_O + \mathcal{M}_N\mathcal{S}_N = \Gamma_g$. From N_b, C_O and C_N the bubble volume v_b is readily obtained,

$$v_b = \frac{(C_O + C_N)\mathcal{R}T_g}{p_g N_b} \tag{23}$$

2.4 Liquid chemistry model

We describe here the water chemistry model used by Wüest *et al*,[11] slightly modified so as to account for oxygen demand. The water chemical variables are the molar concentrations of dissolved oxygen, C_{dO}, and dissolved nitrogen, C_{dN}, together with the biochemical oxygen demand modeled as a scalar field, L. The units of L are kg per cubic meter of mixture. The balance equations are

$$\frac{\partial C_{dO}}{\partial t} + u_\ell \cdot \nabla C_{dO} = \mathcal{S}_{dO} + div\left(\frac{\mu_T}{\rho_\ell Sc_\ell}\nabla C_{dO}\right) \tag{24}$$

$$\frac{\partial C_{dN}}{\partial t} + u_\ell \cdot \nabla C_{dN} = \mathcal{S}_{dN} + div\left(\frac{\mu_T}{\rho_\ell Sc_\ell}\nabla C_{dN}\right) \tag{25}$$

$$\frac{\partial L}{\partial t} + u_\ell \cdot \nabla L = -(K_1 + K_3)L + div\left(\frac{\mu_T}{\rho_\ell Sc_\ell}\nabla L\right) \tag{26}$$

where u_ℓ, the mean liquid velocity, is assumed equal to the mixture velocity u_m and just one turbulent Schmidt number for the liquid's chemistry has been used, Sc_ℓ (usually 0.83). The constants K_1 and K_3 are given by Chapra.[14] We have taken $K_1 = 3.47 \times 10^{-6}$ s^{-1}, $K_2 = 6.94 \times 10^{-6}$ s^{-1}.

The source of dissolved oxygen depends on the exchange with gaseous oxygen, $\mathcal{S}_O$, and on the biochemical demand L following

$$\mathcal{S}_{dO} = -\mathcal{S}_O - \frac{K_1}{\mathcal{M}_O}L \tag{27}$$

while for nitrogen just the gas-liquid exchange was considered, i.e.,

$$\mathcal{S}_{dN} = -\mathcal{S}_N \tag{28}$$

The gaseous exchange is here discussed for oxygen, the case of nitrogen being analogous. It is clear that the net exchange is $\mathcal{S}_O = \mathcal{A}_b F_O$, where $\mathcal{A}_b$ is the interfacial area density and F_O the mean molar surface flux of oxygen, defined positive when flowing from liquid to gas. A typical model for F_O is $F_O = h_m(C_{dO} - C_{dO,I})$, where h_m is the mass transfer coefficient and $C_{dO,I}$ is the concentration of dissolved oxygen at the gas-liquid interface. Assuming local thermodynamic equilibrium at the interface, $C_{dO,I} = K_O p_O$, with K_O the Henry's constant and p_O the partial pressure of oxygen inside the bubble, $p_O =$

$p_g C_O/(C_O + C_N)$. The assumption that the gas inside the bubble has uniform oxygen concentration is implicit in the previous model.

Assuming bubbles to be spherical and of uniform size at each point, $\mathcal{A}_b = (36\pi)^{\frac{1}{3}} v_b^{\frac{2}{3}} N_b$, and from (23) $N_b = (C_O + C_N)\mathcal{R}T_g/(p_g v_b)$, so that $\mathcal{A}_b = (36\pi/v_b)^{\frac{1}{3}}\mathcal{R}T_g(C_O + C_N)/p_g$. The identity, again for spheres, $(36\pi/v_b)^{\frac{1}{3}} = 3/r_b$ leads to the final expressions, for oxygen and nitrogen,

$$\mathcal{S}_O = \frac{3\mathcal{R}T_g(C_O + C_N)h_m}{p_g r_b}\left(C_{dO} - K_O\ p_g \frac{C_O}{C_O + C_N}\right) \tag{29}$$

$$\mathcal{S}_N = \frac{3\mathcal{R}T_g(C_O + C_N)h_m}{p_g r_b}\left(C_{dN} - K_N\ p_g \frac{C_N}{C_O + C_N}\right) \tag{30}$$

where the mass transfer coefficient h_m is assumed to be the same for both species. It is expressed as a function of the bubble radius, varying linearly between zero (for $r_b = 0$) and 4×10^{-4} m/s (for $r_b = 6.67 \times 10^{-4}$ m) and leveling off at that value for larger bubbles. We refer to Wüest *et al* (1992) for further details. Values for Henry's constant at 20°C are taken as $K_O = 1.3516$ mol m^{-3} bar^{-1} and $K_N = 0.6788$ mol m^{-3} bar^{-1}.

2.5 Variants of the gas-phase model

The main variant we discuss here with respect to the basic gas-phase model is to replace the algebraic equation (17) with the gas momentum equation (4). Rearranging the terms so as to get an equation for the relative velocity $u_r = u_g - u_\ell$, using the mass conservation equation and neglecting the diffusive term and the momentum transfer due to mass transfer one gets

$$\begin{aligned}
(\rho_g + C_{vm}\rho_\ell)\left[\frac{\partial u_r}{\partial t} + u_g \cdot \nabla u_r\right] + \sigma u_r &= -\nabla p + (\rho_\ell - \rho_g) g\mathbf{k} \\
\text{turbulent dispersion} \rightarrow &\quad -\frac{\sigma \mathcal{D}_b}{\alpha_g}\nabla\alpha_g \\
\text{lift} \rightarrow &\quad -C_L\,\rho_\ell\,u_r \times (\nabla \times u_\ell) \\
\text{remainder of inertia} \rightarrow &\quad -\rho_g \frac{\partial u_\ell}{\partial t} - C_{vm}\,\rho_\ell\,u_r \cdot \nabla u_\ell
\end{aligned} \tag{31}$$

where the first term on the left is one part of the inertia term, accounting for virtual mass through the coefficient C_{vm}, while the second term is due to drag, with $\sigma = 3\rho_\ell C_D |u_r|/(8 r_b)$, C_D being the drag coefficient obtained from

$$C_D = \frac{24}{Re}\left(1 + 0.1 Re^{0.75}\right) \tag{32}$$

On the right we find first the pressure and buoyancy terms, and we have also identified the terms corresponding to *turbulent dispersion forces* and *lift forces*. One thus has two alternatives for incorporating turbulent dispersion, either in the gas mass equation through $\mathcal{D}_g$

or in the gas momentum equation through $\mathcal{D}_b$. We also define a bubble Schmidt number by

$$\mathcal{D}_b = \frac{\mu_T}{\rho_\ell Sc_b} \tag{33}$$

3 NUMERICAL IMPLEMENTATION

The numerical implementation of the CFD model is performed with finite elements. Bilinear interpolation is used in the simulations discussed here. The equations are advanced in time decomposing the time step into several substeps, as follows:

1. **Pressure gradient projection:** We are using an equal order formulation stabilized by pressure gradient projection.[36–39] The first step is the orthogonal projection of the pressure gradient onto the velocity interpolation space. This is accomplished using the lumped mass matrix.

2. **Navier-Stokes system:** With the calculated projected pressure gradient and the turbulent viscosity and effective density from the previous time step, the system (13)-(14) is solved with a backward-Euler scheme. The convection term is linearized in the usual way, $\rho^{*n}(u_m^n \cdot \nabla)u_m^{n+1}$. The SUPG method is used as upwinding technique for the convection terms in *all* substeps.

3. $k-\epsilon$ **system:** The standard equations for k and ϵ are solved using the already computed velocity field. The specific implementation, in particular concerning the treatment of spurious negative values of the variables, can be found in the article by Lew *et al.*[17]

4. **Bubbles' slip velocity evaluation:** Using (23), with C_O, C_N and N_b from the previous time step, the bubble radius is calculated and the bubbles' slip velocity w_b evaluated at all nodes of the mesh. On the other hand, if the gas-momentum equation is used, at this step (31) is solved for the relative velocity u_r.

5. **Gaseous concentrations variables:** Computing the gas velocity as $u_g = u_m + \mathbf{k}\, w_b$ (or alternatively $u_g = u_\ell + u_r$), the equations for N_b (16), C_O (21) and C_N (22) are advanced in time, with the source terms evaluated at the previous time step. The remaining terms are treated implicitly in time, with one exception: Let f be a gas variable, then, since u_g is not necessarily solenoidal, there appears a term $f\ div\ u_g$. This term is treated either implicitly or explicitly depending on whether $div\ u_g$ is positive or negative, respectively; and the condition is applied pointwise through the Gaussian-points do-loop. Significant stability and robustness was gained with this simple trick.

6. **Liquid chemistry variables:** Finally, equations (24)-(26) are advanced in time. Though updated values of C_O, C_N and N_b are available, the sources (29)-(30) are

computed with values frozen at the previous time step, so that they are consistent with those used at the previous substep and (27)-(28) hold exactly. This makes the algorithm globally conservative.

4 NUMERICAL RESULTS

4.1 Description of the wastewater-reservoir tests

The simulations reported here are performed at prototype scale, for the case of McCook Reservoir in Chicago, with a water depth of 77 m. Atmospheric air is injected at the bottom through a circle of diameter 65 cm, with a molar composition of 21 % oxygen and 79 % nitrogen, at a volumetric rate Q_g (at the bottom pressure). Ambient concentrations are 1 mg/liter of dissolved oxygen and 0.28 mg/liter of dissolved nitrogen. The biochemical oxygen demand is taken as 30 mg/liter. Typical conditions are $Q_g = 1.2$ liter/s, with a bubble radius of 2.5 mm, but simulations under other conditions have also been performed.

The CFD simulations consider axisymmetric conditions, so that a 2D mesh of 8000 bilinear quadrilaterals is adopted. This mesh is called COARSE mesh, the minimum element sizes are $\Delta r = 14$ mm and $\Delta z = 32$ mm (see Fig. 1). The FINE mesh used in the convergence study is obtained by dividing each quadrilateral into four, so that the grid size is halved.

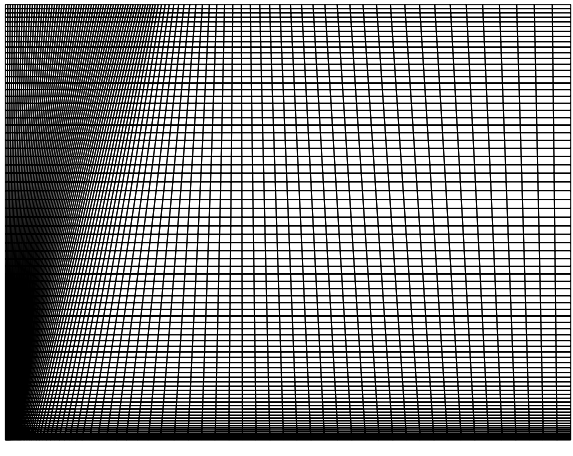

Figure 1: Mesh used in calculations at reservoir's scale.

The domain extends horizontally up to a radius of 100 m, which is large enough for finite-size effects to be negligible (the downwards counterflow at the exterior boundary has a velocity of 0.4 mm/s, less than 0.3 % of the plume's velocity). Symmetry conditions were imposed at the artificial vertical boundary. The same was done at the top boundary

for the liquid phase, while for the gas phase the top surface is an outflow boundary. The logarithmic smooth-wall law was imposed at the bottom. Since we are analyzing processes in the plume's vicinity, simulations were run for about 3000 seconds of simulated time (time steps used were in the range 1-4 s), for which all the near-plume variables are stable. The full establishment of the far-field flow for this geometry takes more than ten times that value, but the plume's quantities discussed here are not affected.

4.2 CFD results

Let us overview some sample CFD results at nominal conditions $Q_g = 1.2$ liter/s, inlet bubble radius of 2.5 mm. In Fig. 2 the velocity field is depicted. The conical shape of the plume is evident, up to a depth of about 15 m ($z = 52$ m) where the effect of the surface becomes significant and lateral spreading begins. This surface-affected depth (about 25 % of total depth) is in agreement with observations by Ditmars & Cederwall.[3]

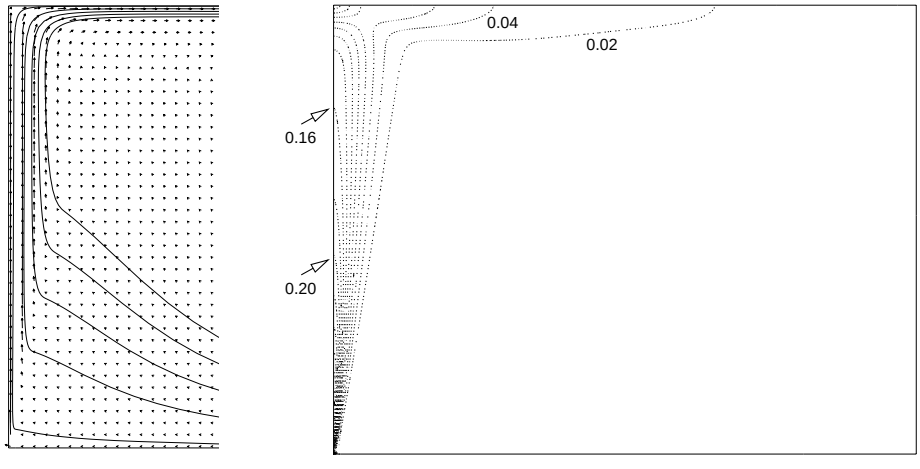

(a) (b)

Figure 2: Velocity field u_m obtained with the CFD code. $Q_g = 1.2$ liter/s and $r_b = 2.5$ mm at the inlet. (a) Velocity vectors and a few selected streamlines. (b) Equispaced velocity-modulus contours, contour interval is 0.02 m/s. The maximum of $|u_m|$ over the domain is 0.425 m/s.

Figure 3 depicts some CFD results concerning the gaseous phase. In part (a) of the figure the volume fraction α_g is shown. Practically all the plume has $\alpha_g < 10^{-2}$. Part (b) shows the bubble radius. In part (c) the molar fraction of oxygen in the bubbles' gas is shown. The simulation predicts that the gas leaving from the surface (which in fact is only 11% of the injected gas) is largely oxygen-depleted to about 6%. Notice also the horizontal gradients in the gas composition; this affects the partial pressure of each

species inside the bubbles and thus the mass transfer at the interface (see Eqs. 29 and 30).

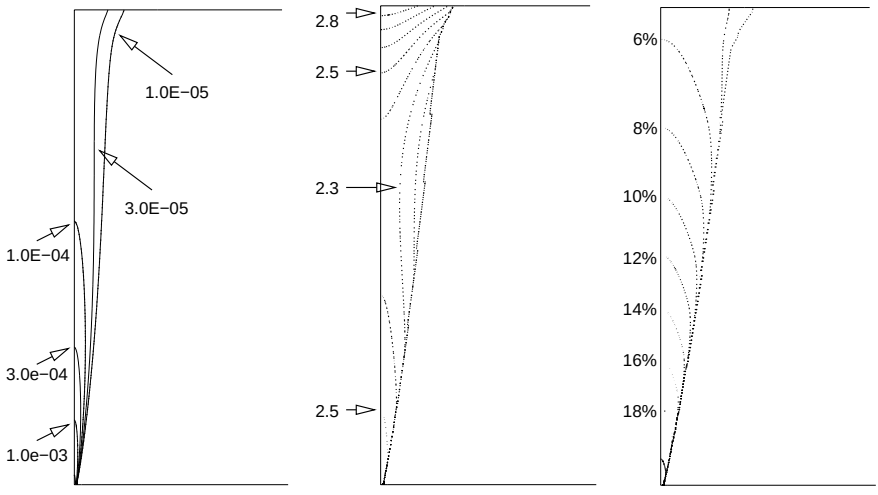

Figure 3: Results of the CFD code for the gaseous phase variables. (a) Volume fraction α_g. (b) Bubble radius in mm (only calculated where $N_b > 10$ bubbles/m^3). (c) Molar fraction of oxygen in the gas.

To check grid-independence of the results a run with the same nominal conditions was run with mesh FINE, which has 200 × 160 quadrilaterals and half the mesh size of the previous run. In Fig. 4 we show comparisons of the results obtained with both meshes along the centerline. Not only good agreement is found in the velocity and oxygen concentration, but also in the turbulent variables (k and ϵ). In the same figure the results at $t = 2000$ s are shown, proving the steadiness of the flow variables at the plume.

4.3 Comparison of results of CFD and 1D codes

Most important concerning aeration plumes are global parameters such as the fraction of the injected air that dissolves in the water and the so-called gas holdup, defined as the amount of gas present in the water column at each given instant. For plumes with inlet bubble radius of 2.5 mm these quantities are plotted as functions of Q_g in Fig. 5. In part (a) we compare the fraction of air dissolved (FAD) as calculated with the CFD code to that obtained with the 1D model described elsewhere.[15] A quite good agreement is observed over the whole range 0.1–3 liter/s. The decrease in FAD with Q_g is due to the smaller residence time of each bubble in the water column, due to the increase in the liquid's velocity with Q_g. This is coherently predicted by both models. For $Q_g > 2$ the

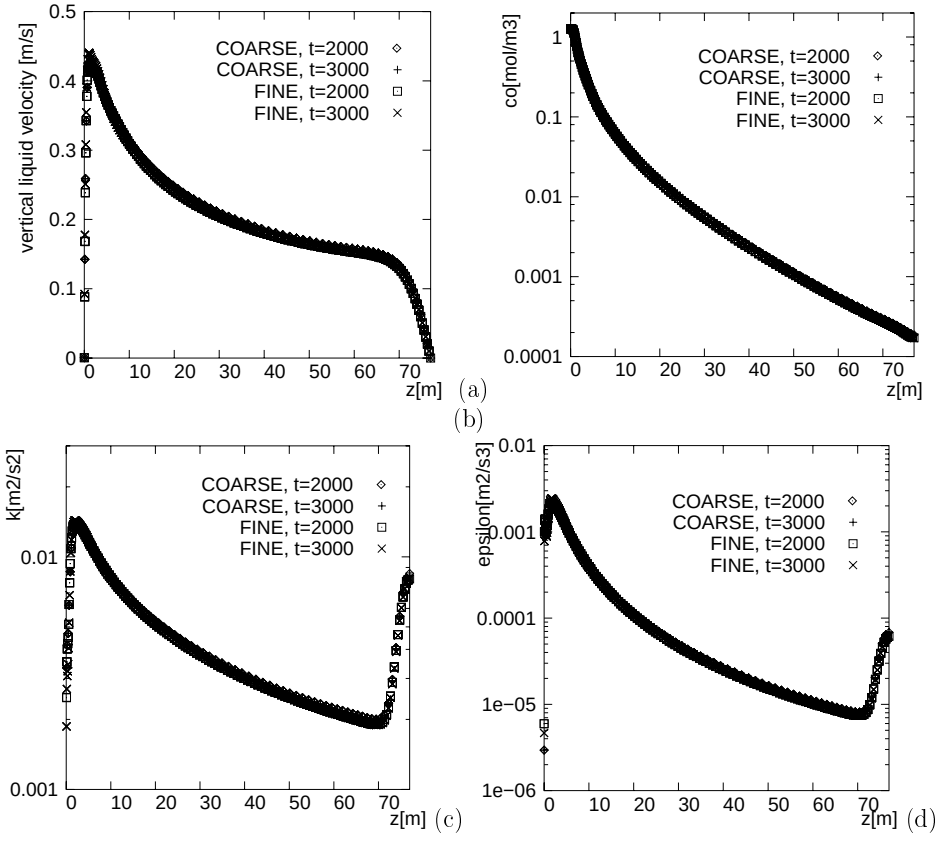

Figure 4: A comparison of the numerical results obtained using meshes FINE and COARSE, for instants $t = 2000$ s and $t = 3000$ s, so as to check grid-independence and steadiness of the solution. We plot, as functions of z, the following variables along the centerline: (a) Vertical liquid velocity, (b) gaseous oxygen concentration, (c) k, (d) ϵ.

FAD in the CFD results tends to level off, while the 1D results keep decreasing with Q_g, but both results differ by less than a few percents so that this discrepancy was not further studied. In part (b) a similar comparison is shown for oxygen and nitrogen holdups, with good agreement.

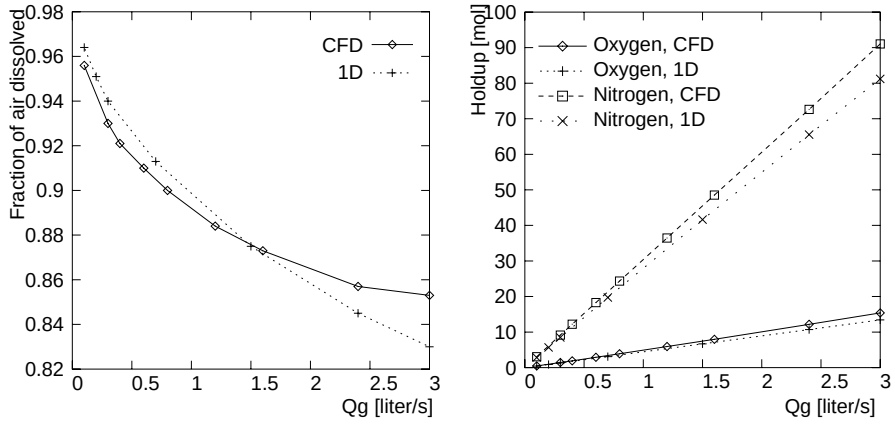

(a) (b)

Figure 5: Comparison of global parameters obtained from the CFD and 1D results. (a) Fraction of the injected gas that dissolves in the plume. (b) Gas holdup, discriminated by species. Both as functions of Q_g.

We compare the mean vertical liquid velocity in the plume as calculated from the CFD results to those predicted by the 1D model in Fig. 6 (a), for $Q_g = 0.3$, 1.2 and 3.0 liter/s. The agreement is quite good except in two regions: The first few meters and near the surface. The latter is natural, since the free-surface condition is not accounted for in the 1D model. The discrepancies in the first few meters, on the other hand, are explained by the different flow geometries near the diffuser assumed by the two models.

In Fig. 6 (b) we compare predictions of the CFD and 1D models for bubbles' radius variations with z. The CFD result shown is the bubble-flux-weighted horizontal mean

$$\overline{r_b}(z) = \frac{\int_{S(z)} r_b N_b (u_m \cdot \mathbf{n} + w_b) dS}{\int_{S(z)} N_b (u_m \cdot \mathbf{n} + w_b) dS}$$

One observes that the r_b predicted by the CFD model is larger than that from the 1D model. This difference must be regarded as a discrepancy between the models. However, it is not observed to be larger than 5–10 % for the cases analyzed.

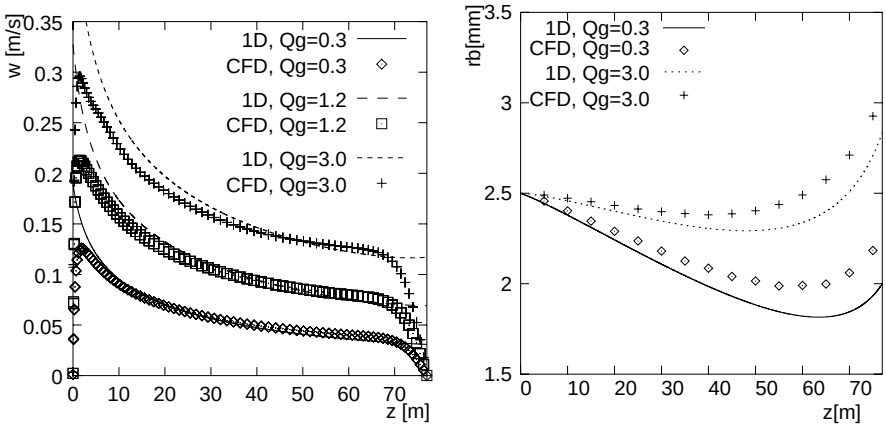

(a) (b)

Figure 6: Comparison of vertical profiles of (a) mean liquid velocity (denoted by w in the text) and (b) mean bubble radius, for several values of Q_g.

4.4 Entrainment coefficient

The entrainment coefficient was evaluated from the plume's volumetric flux, momentum flux, width and velocity. This is shown for a particular case ($Q_g = 1.2$ liter/s) in Fig. 7, but the behavior is quite the same in all the runs made. The values are of the order of 0.1, decreasing from the diffuser upwards. Notice that the analysis was carried out between $z = 15$ m and $z = 45$ m, where no effects of the bottom wall or of the free surface is noticeable.

Milgram[10] obtained quite similar values in his experiments in a 50-m deep reservoir with $Q_g = 4.1$ liter/s ($\alpha \simeq 0.085$, after multiplying his values by $\sqrt{2}$ because of a difference in the definition of α). Milgram measured entrainments coefficients that increased with z, contrary to our CFD results, but most of his data are at extremely high gas flow rates. The data of Fannelop & Sjoen as analyzed by Milgram[10] also exhibit entrainment coefficients that agree with our CFD results. For $Q_g = 2.5$ liter/s they obtained $\alpha \simeq 0.1$, increasing up to $\alpha = 0.14$ for $Q_g = 12$ liter/s. Remarkably, their data also show entrainment coefficients that *decrease* with z, particularly for the lower flow rates. Other available values of α also fall in the range 0.07–0.12.[3,40] Entrainment coefficients obtained from the CFD code are thus in reasonable agreement with experimental data, notwithstanding the simplicity of the turbulent model employed.

Since the radial profiles of α_g and of the vertical component of u_m are almost exactly Gaussian, it is easy to evaluate the ratio of the two widths, denoted by $\lambda(z)$, from the CFD results. As shown in Fig. 7, a fairly constant λ of approximately 0.7 is obtained.

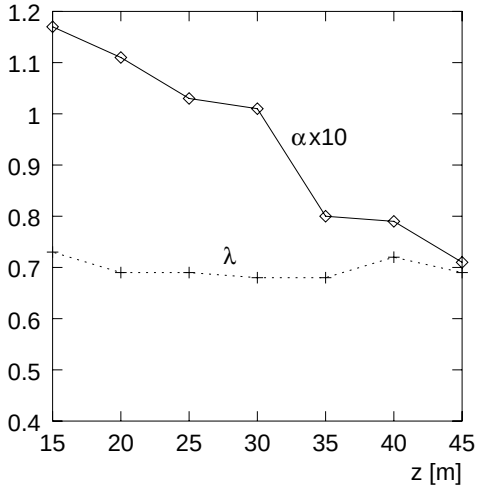

Figure 7: Values of α and λ as obtained from the CFD results, as functions of z, for the simulation with $Q_g = 1.2$ liter/s.

This is in agreement with the values reported by Milgram[10] and by Tekeli & Maxwell.[40]

4.5 Simulation of an experimental tank. Assessment of forces

The purpose of this section is to compare the performance of different alternatives to represent the turbulent dispersion and to assess the relative influence of the forces in (31). A tank with the geometry shown in Fig. 8 was adopted. Experiments are being carried out in this tank and comparisons with the simulations will be reported in the future. The gas inflow takes place through a diffuser of 0.42 m in diameter. An airflow rate of 1.3 scfm was considered, together with a bubble size of 2.5 mm. A mesh of 4900 quadrilateral elements was used (see Fig. 8).

Let's begin comparing the performance of the model which computes the gas velocity from (17), which we denote as Test 1 in Table 1, with that which solves the gas momentum equation (31), but including only the forces of drag and buoyancy (Test 2 in Table 1). This allows us to address any discrepancy in the prediction of the gas velocity and its relation with the liquid mean flow field. In that regard, the vertical velocity, turbulent kinetic energy and void fraction were chosen as representative variables to base the comparison, for two heights above the diffuser (3 and 6 m). Figure 9 shows that the liquid's velocities computed in Test 1 are larger than those of Test 2. A similar trend is observed in terms of the turbulent kinetic energy (Figure 10). For the void fraction the larger differences are located far from the centerline (Figure 11). The reason of the discrepancies is that the

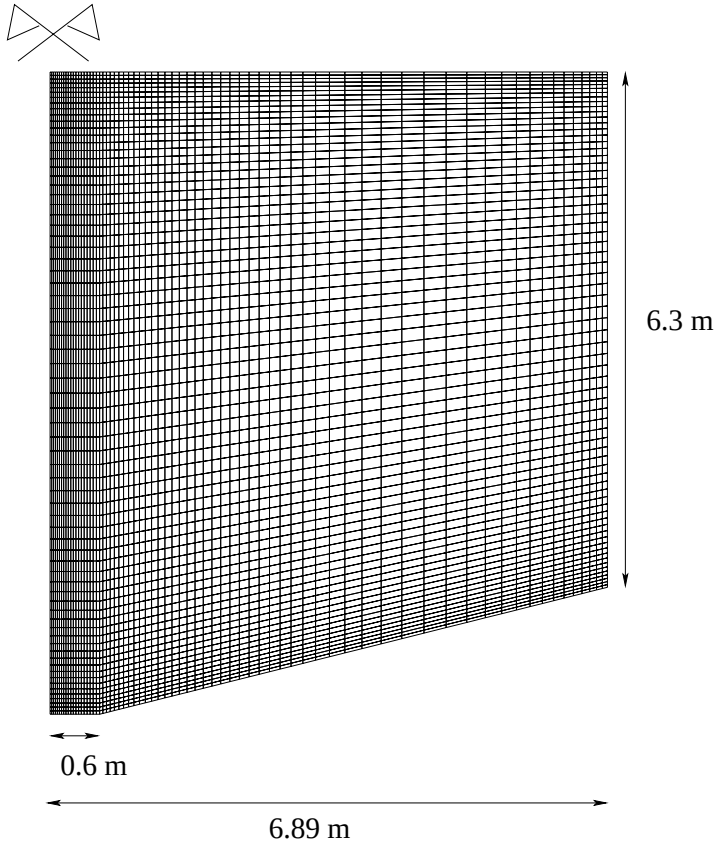

Figure 8: Geometry and mesh for the simulation of the experimental tank.

gas slip velocities in the bubble core predicted in Test 2 (not shown herein) are about 0.4 m/s, much larger than the 0.23 m/s predicted in Test 1. This is not surprising, since the relation (32) is valid for small bubbles[41,42] but may underestimate C_D for intermediate ones.[33] With all, it is fair to recognize that the differences in the predictions of the main flow variables are well below 15 %, which is of the order of the empirical errors involved.

Next step consisted in investigating to what extent it is equivalent to add turbulent dispersion via the coefficients $\mathcal{D}_g$, which enters the mass-conservation equation, or $\mathcal{D}_b$ which enters the momentum equation in the turbulent-dispersion force. For this, we fixed the *total* effective Schmidt number,

$$Sc_t = \left(\frac{1}{Sc_g} + \frac{1}{Sc_b} \right)^{-1}$$

to 0.83 so as to make things comparable. Several tests were done covering a wide range of cases, but only one representative result is presented as Test 3. Test 2 represents the test in which all the dispersion is undertaken by $\mathcal{D}_g$, while in Test 3 $\mathcal{D}_g$ only accounts for 1/4 of the dispersion and $\mathcal{D}_b$ for the remaining 3/4. In Figs. 9-11 it is observed that for this case practically no differences arise. Turbulent dispersion can thus be treated within the gas mass conservation equation, which is numerically more stable.

The third step consisted in comparing the results of the model activating one force (other than the drag force) at a time. Since the lift force points in a direction perpendicular to the local mean flow, changes are expected. Also, changes could be expected when introducing the virtual mass force, as pointed out by Smith.[25]

Two tests were undertaken: Test 4 includes only the lift force whereas Test 5 considers only the virtual mass force. The values adopted for the coefficients included in the lift and virtual mass forces were 0.1 and 0.5, respectively. Figures 9-11 show that the differences between Tests 4 and 5, and Test 2 are relatively small.

All the above tests were done taking $\rho^* = \rho_m$ in (13)-(14). Test 6 is equivalent to Test 2 but taking $\rho^* = \rho_\ell$. Again, no significant changes appear.

Summarizing, the simulations show that the basic gas-phase model discussed in the previous sections has no major differences with more "mechanistic" models such as (31). We expect this to be true for *large* and *dilute* plumes, as discussed in Section 2 (see also[15]).

4.6 Simulation of spontaneous plume wandering

The last numerical example we discuss here is that of a flat bubble column with a moderate gas throughflow, which is thoroughly detailed by Becker *et al.*[21] The importance of this flow setup is that it spontaneously bifurcates to a quasi-periodic motion with large-scale vortices continuously changing location in time at low frequencies.[22] It constitutes a stringent test to numerical methods because overdiffusive schemes do not capture the bifurcation and yield steady-state solutions that are just numerical artifacts.[22] The geometry consists of a rectangular prism with width 50 cm, depth 8 cm and height 150 cm.

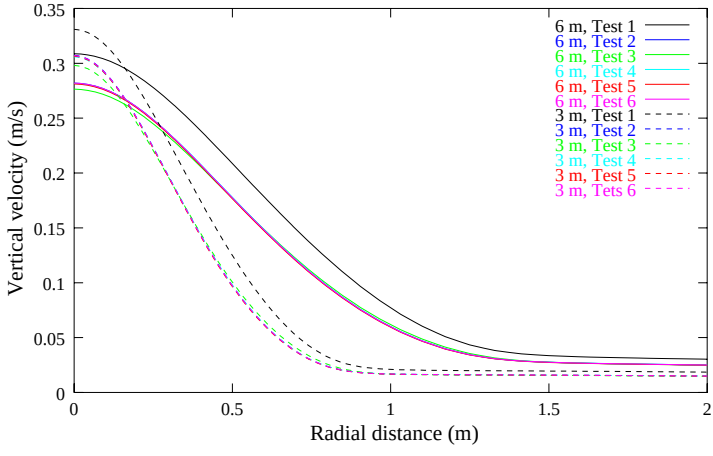

Figure 9: Comparison of profiles, at $z = 3$ and 6 m above the diffuser, of the liquid vertical velocity for the different tests. All tests except 1 and 3 are practically superposed.

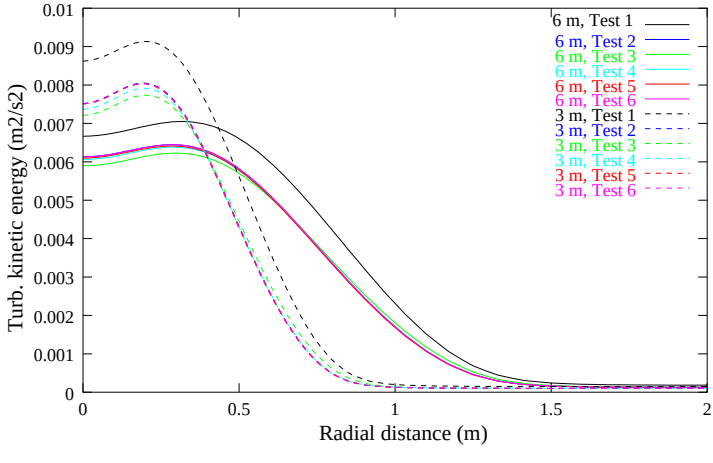

Figure 10: Comparison of profiles, at $z = 3$ and 6 m above the diffuser, of the turbulent kinetic energy for the different tests. All tests except 1 and 3 are practically superposed.

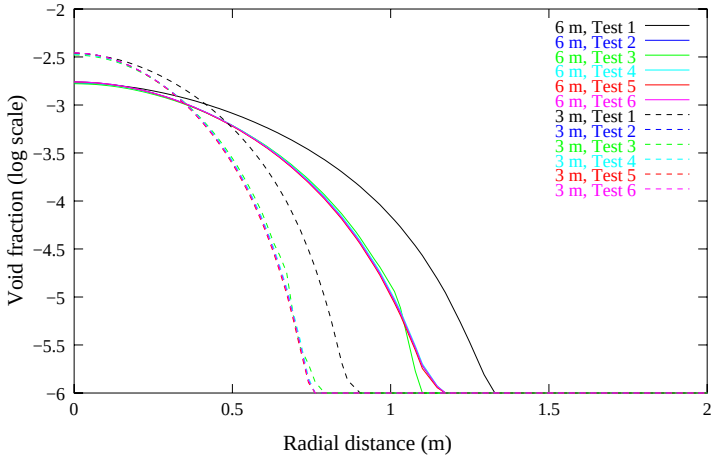

Figure 11: Comparison of profiles, at $z = 3$ and 6 m above the diffuser, of the void fraction for the different tests. All tests except 1 and 3 are practically superposed.

Tests	1	2	3	4	5	6
Sc_g	0.83	0.83	3.32	0.83	0.83	0.83
Sc_b	NA	∞	1.107	∞	∞	∞
Lift force	NA	NO	NO	YES	NO	NO
Virtual mass force	NA	NO	NO	NO	YES	NO
Gas velocity equation	(17)	(31)	(31)	(31)	(31)	(31)
$\rho^* =$	ρ_m	ρ_m	ρ_m	ρ_m	ρ_m	ρ_ℓ
Time step (s)	0.4	0.1	0.1	0.1	0.1	0.1

Table 1: Summary of the tests performed

A gas distributor is mounted at the bottom at a distance of 15 cm from the left side of the column, and injects 0.0264 liters of gas per second.

In Fig. 12 we show the successive snapshots of the gas concentration field on the mid-plane, with a time interval of 5 seconds. The phenomenon of "plume wandering" is well captured by the proposed methodology.

5 CONCLUSIONS

In this article we have derived a multidimensional mathematical model for dilute bubbly two-phase plumes from the two-fluid model equations. The necessary approximations were discussed and later shown to hold in some cases of interest. The closure relations, in particular concerning Reynolds stresses and turbulent dispersion of the bubbles, were taken from simple models that are reasonable in view of the present knowledge on the subject.

Further on, a mass transfer model was presented that coincides with that of the integral model proposed by Wüest *et al* (1992).[11] By coupling this model to the aforementioned two-phase flow model a CFD version of the 1D model was obtained.

A set of runs was performed for the conditions of a deep, biochemically active reservoir with a single, isolated plume using both a 1D model and the proposed CFD code. By direct comparison good agreement between both models is observed for the most relevant variables such as gas dissolution rates, gas holdup, liquid's velocity and bubbles' radius. In addition, the entrainment coefficient derived from the CFD results was shown to be consistent with available experimental results. The same was shown for the ratio of the bubbly core width to the plume width.

Our objective has been to present a fully consistent picture of 1D and CFD models for bubble plumes through both mathematical derivation and direct comparison of numerical results. From the good agreement, CFD models can be seen as natural extensions of integral models which have been developed and experimentally verified by the environmental fluid dynamics community over the years. This extension of 1D models to CFD ones is obviously necessary to address many technologically relevant phenomena, such as plume-plume interactions and plumes confined within complex boundaries or immersed in complex crossflows.

In these more complex conditions more elaborate models may prove necessary. One such model, with a complete momentum equation for the gas phase has also been presented, and the effect of the different forces on the behavior of a large-scale bubble plume has been assessed. It has been confirmed that the two alternative methods of treating turbulent dispersion yield undistinguishable results for the cases considered, that the lift and virtual mass forces are negligible, and that the proposed method is able to capture the experimentally-observed spontaneous bifurcation to a quasi-periodic flow in a confined bubble plume.

ACKNOWLEDGMENTS: The financial support of the U. S. Army Corps of En-

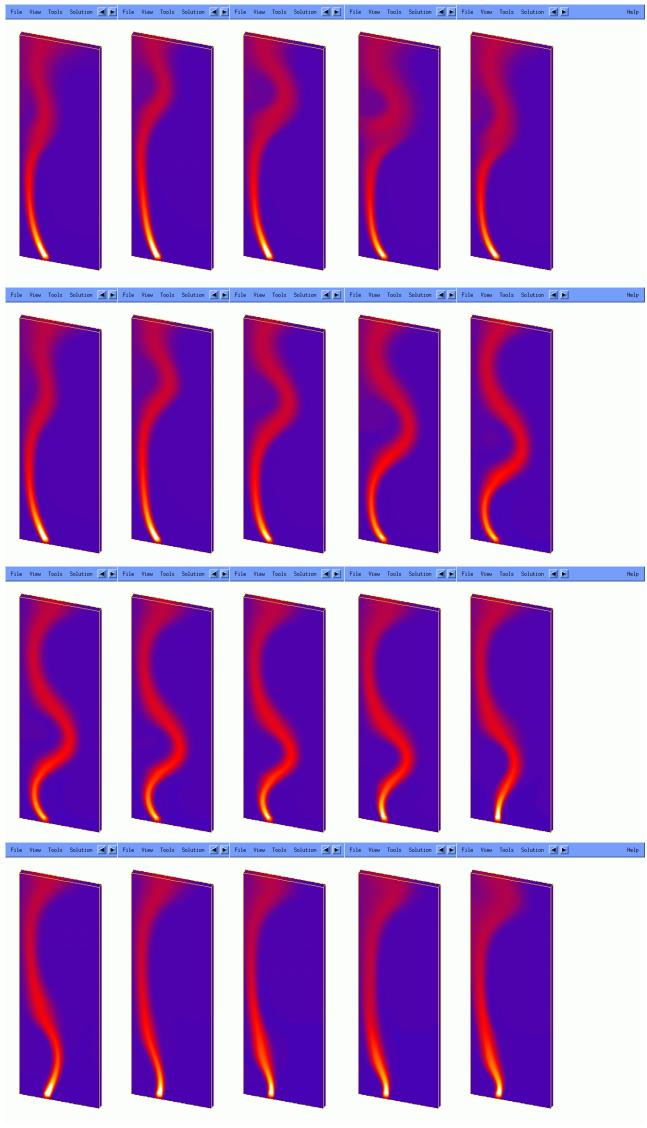

Figure 12: Successive snapshots of the gas concentration field on the mid-plane of the confined bubble plume. Time interval between snapshots is 5 seconds.

gineers (Chicago District), through research contract DACA 88-98-D-005-15 is gratefully acknowledged. FAB is on leave from INA, Argentina. GCB and EAD also belong to CONICET, Argentina.

REFERENCES

[1] G. Ashton. Numerical simulation of air bubbler systems. *Can. J. Civ. Eng.*, **5**, 231–238 (1978).

[2] P. Bulson. The theory and design of bubble breakwaters. *Proc. 11th Conf. Coastal Engng., London*, pages 995–1015 (1968).

[3] J. Ditmars and K. Cederwall. Analysis of air-bubble plumes. In *Proc. 14th Coastal Eng. Conf., Copenhagen*, pages 2209–2226. ASCE, (1974).

[4] G. Taylor. The action of a surface current used as a breakwater. *Proc. Roy. Soc.*, **A231**, 466–478 (1955).

[5] S. Schladow. Bubble plume dynamics in a stratified medium and the implications for water quality amelioration in lakes. *Water Resources Res.*, **28**, 313–321 (1992).

[6] T. Asaeda and J. Imberger. Structure of bubble plumes in linearly stratified environments. *J. Fluid Mech.*, **249**, 35–57 (1993).

[7] Ch. Lemckert and J. Imberger. Energetic bubble plumes in arbitrary stratification. *J. Hydraulic Eng.*, **119**, 680–703 (93).

[8] Joint Task Force of the Water Pollution Control Federation and the American Society of Civil Engineers, editors. *Aeration: A wastewater treatment process.* ASCE - Manuals and Reports on Eng. Practice No. 68. WPCF - ASCE, (1988).

[9] T. McDougall. Bubble plumes in stratified environments. *J. Fluid Mech.*, **85**, 655–672 (1978).

[10] J. Milgram. Mean flow in round bubble plumes. *J. Fluid Mech.*, **133**, 345–376 (1983).

[11] A. Wüest, N. Brooks, and D. Imboden. Bubble plume modeling for lake restoration. *Water Resources Research*, **28**, 3235–3250 (1992).

[12] J. Turner. Turbulent entrainment: the development of the entrainment assumption, and its application to geophysical flows. *J. Fluid Mech.*, **173**, 431–471 (1986).

[13] D. Drew and S. Passman. *Theory of Multicomponent Fluids*, volume 135 of *Applied Mathematical Sciences*. Springer, (1998).

[14] S. Chapra. *Surface water-quality modeling*. Mc Graw–Hill, (1997).

[15] G. C. Buscaglia, F. A. Bombardelli, and M. H. García. Numerical modeling of large-scale bubble plumes accounting for mass transfer effects. *Int. J. Multiphase Flow*, **to appear** (2002).

[16] D. Wilcox. *Turbulence Modeling for CFD*. DCW Industries, La Cañada, California, (1998).

[17] A. J. Lew, G. C. Buscaglia, and P. M. Carrica. A note on the numerical treatment of the k-epsilon turbulence model. *International Journal of Computational Fluid Dynamics*, **14**, 201–209 (2001).

[18] Y. Sato, M. Sadatomi, and K. Sekoguchi. Momentum and heat transfer in two-phase

bubble flow - I. *Int. J. Multiphase Flow*, **7**, 167–177 (1981).

[19] R. Mudde and O. Simonin. Two- and three-dimensional simulations of a bubble plume using a two-fluid model. *Chem. Eng. Sci.*, **54**, 5061–5069 (1999).

[20] P. Viollet and O. Simonin. Modelling dispersed two-phase flows: Closure, validation and software development. *Appl. Mech. Rev.*, **47**(2), 80–84 (1994).

[21] S. Becker, A. Sokolichin, and G. Eigenberger. Gas-liquid flow in bubble columns and loop reactors: Part II. Comparison of detailed experiments and flow simulations. *Chem. Eng. Sci.*, **49**, 5747–5762 (1994).

[22] A. Sokolichin and G. Eigenberger. Applicability of the standard $k - \epsilon$ turbulence model to the dynamic simulation of bubble columns: Part I. Detailed numerical simulations. *Chem. Eng. Sci.*, **54**, 2273–2284 (1999).

[23] O. Borchers, C. Busch, A. Sokolichin, and G. Eigenberger. Applicability of the standard $k - \epsilon$ turbulence model to the dynamic simulation of bubble columns: Part II. Comparison of detailed experiments and flow simulations. *Chem. Eng. Sci.*, **54**, 5927–5935 (1999).

[24] D. Pfleger, S. Gomes, N. Gilbert, and H. Wagner. Hydrodynamic simulations of laboratory scale bubble columns fundamental studies of the eulerian-eulerian modeling approach. *Chem. Eng. Sci.*, **54**, 5091–5099 (1999).

[25] B. Smith. On the modelling of bubble plumes in a liquid pool. *Appl. Math. Modell.*, **22**, 773–797 (1998).

[26] M. Malin and D. Spalding. A two-fluid model of turbulence and its application to heated plane jets and wakes. *PCH PhysicoChemical Hydrodynamics*, **5 (5/6)**, 339–362 (1984).

[27] J. Grevet, J. Szekely, and N. El-Kaddah. An experimental and theoretical study of gas bubble driven circulation systems. *Int. J. Heat Mass Transfer*, **25**, 487–497 (1982).

[28] J. Woo, J. Szekely, A. Castillejos, and J. Brimacombe. A study on the mathematical modeling of turbulent recirculating flows in gas-stirred ladles. *Metall. Trans. B*, **21B**, 269–277 (1990).

[29] S. Joo and R. Guthrie. Modeling flows and mixing in steelmaking ladles designed for single- and dual-plug bubbling operations. *Metall. Trans. B*, **13B**, 765–778 (1992).

[30] J. Hua and C.-H. Wang. Numerical simulation of bubble-driven liquid flows. *Chem. Eng. Sci.*, **55**, 4159–4173 (2000).

[31] J. Morchain, C. Maranges, and C. Fonade. CFD modelling of a two-phase jet aerator under influence of a crossflow. *Water Research*, **34**, 3460–3472 (2000).

[32] W. Haberman and R. Morton. An experimental study of bubbles moving in liquids. *Proc. Am. Soc. Civ. Eng.*, **80**, 379–427 (1954).

[33] R. Clift, J. Grace, and M. Weber. *Bubbles, drops and particles.* Academic Press, (1978).

[34] P. Carrica, F. Bonetto, D. Drew, and R. Lahey Jr. The interaction of background ocean air bubbles with a surface ship. *Int. J. Numerical Methods in Fluids*, **28**, 571–

600 (1998).

[35] F. Moraga, A. Larreteguy, D. Drew, and R. Lahey Jr. Assessment of turbulent dispersion models for bubbly flows. *submitted*, (2001).

[36] R. Codina and J. Blasco. A finite element formulation for the stokes problem allowing equal velocity-pressure interpolation. *Comp. Meth. in Appl. Mech. and Engrg.*, **143**, 373–391 (1997).

[37] R. Codina and J. Blasco. Stabilized finite element method for the transient navier-stokes equations based on a pressure gradient projection. *Comp. Meth. in Appl. Mech. and Engrg.*, **182**, 277–300 (2000).

[38] G. Buscaglia, F. Basombrío, and R. Codina. Fourier analysis of an equal-order incompressible flow solver stabilized by pressure-gradient projection. *Int. J. Numer. Meth. in Fluids*, **34**, 65–92 (2000).

[39] R. Codina, J. Blasco, G. Buscaglia, and A. Huerta. Implementation of a stabilized finite element formulation for the incompressible navier-stokes equations based on a pressure gradient projection. *Int. J. Numer. Meth. in Fluids*, **37**, 410–444 (2001).

[40] S. Tekeli and W. Maxwell. Behavior of air bubble screens. Civil Eng. Studies, Hydraulic Eng. Res. Series 33, University of Illinois at Urbana-Champaign, (1978).

[41] G. Sridhar and J. Katz. Drag and lift forces on microscopic bubbles entrained by a vortex. *Phys. Fluids*, **7(2)**, 389–399 (1995).

[42] K. Felton and E. Loth. Spherical bubble motion in a turbulent boundary layer. *Phys. Fluids*, **13(9)**, 2564–2577 (2001).